

# Double-semion topological order from exactly solvable quantum dimer models

Yang Qi,<sup>1,\*</sup> Zheng-Cheng Gu,<sup>2,†</sup> and Hong Yao<sup>1,3,‡</sup>

<sup>1</sup>*Institute for Advanced Study, Tsinghua University, Beijing 100084, China*

<sup>2</sup>*Perimeter Institute for Theoretical Physics, Waterloo, Ontario, Canada N2L 2Y5*

<sup>3</sup>*Collaborative Innovation Center of Quantum Matter, Beijing, 100084, China*

We construct a generalized quantum dimer model on two-dimensional nonbipartite lattices including the triangular lattice, the star lattice and the kagome lattice. At the Rokhsar-Kivelson (RK) point, we obtain its exact ground states that are shown to be a fully gapped quantum spin liquid with the double-semion topological order. The ground-state wave function of such a model at the RK point is a superposition of dimer configurations with a nonlocal sign structure determined by counting the number of loops in the transition graph. We explicitly demonstrate the double-semion topological order in the ground states by showing the semionic statistics of monomer excitations. We also discuss possible implications of such double-semion resonating valence bond states to candidate quantum spin-liquid systems discovered experimentally and numerically in the past few years.

PACS numbers: 75.10.Kt, 05.30.Pr

## I. INTRODUCTION

Topological order [1–3] is a key concept with increasing importance in studies for quantum many-body systems, especially for strongly correlated electronic systems. Quantum states with the so-called intrinsic topological order can be characterized by patterns of long-range quantum entanglement [4–6], and feature fractionalized excitations carrying fractional charge and anyonic statistics. Besides being interesting on their own, quantum states with certain topological orders may have interesting applications for fault-tolerant quantum computations [7, 8]. The experimentally observed fractional quantum Hall (FQH) states [9, 10] are seminal examples of the emergence of topological order in strongly correlated electronic systems. The concept of topological orders has been widely used in the studies of quantum spin liquids [11–13] and high- $T_c$  superconductors [1, 14–16].

Quantum dimer models [17] were first introduced to study quantum spin liquids and high- $T_c$  cuprate in the context of short-range resonating valence bond (RVB) states [14, 18]. Later it was shown that on a nonbipartite lattice, the ground state of quantum dimer models described by the Rokhsar-Kivelson (RK) Hamiltonian [19] can realize a particular topological order—the  $Z_2$  topological order [12, 20], which is among the simplest intrinsic topological orders and it is also known as the toric-code topological order [7]. In recent years, more topological orders have been realized systematically in exactly solvable models, *e.g.*, the string-net models [21] and Kitaev models [22]. In the past few years, evidences of gapped quantum spin-liquid ground states were reported in numerical simulations of frustrated spin  $SU(2)$ -symmetric models using the methods

of density matrix renormalization group (DMRG) [23–25] and pseudofermion functional renormalization group (PFFRG) [26], and in experiments on real materials [27]. Short-range RVB wave functions (or, equivalently, dimer wave functions) with  $Z_2$  topological order are often considered as candidate ground states. Nonetheless, recent DMRG studies reported indirect evidence that the  $Z_2$  topological order might not describe the ground state of the kagome spin-1/2 Heisenberg model [28–32].

Therefore, we naturally ask the following question: Can short-range RVB-type wave functions in two-dimensional (2D) support a different topological order than the  $Z_2$  one? Our answer is positive by constructing an exactly solvable Hamiltonian of quantum dimers (or bond singlets) whose ground state has the double-semion topological order [21, 33] instead of the  $Z_2$  or toric-code topological order. Our construction is quite simple as we only change the phase of resonant terms in the original RK Hamiltonian, as follows:

$$H = \sum_{P_\alpha} [(it|P_\alpha\rangle\langle P_{\bar{\alpha}}| + \text{H.c.}) + v(|P_\alpha\rangle\langle P_\alpha| + |P_{\bar{\alpha}}\rangle\langle P_{\bar{\alpha}}|)], \quad (1)$$

where  $P_1 = \triangleleft$ ,  $P_2 = \triangleright$ ,  $P_3 = \nabla$ , and  $P_{\bar{\alpha}}$  is obtained by flipping the dimer configurations of  $P_\alpha$ . Note that in the original RK Hamiltonian [17], the coefficient of resonance terms is  $-t$ . Here, it is changed to  $it$ , which could have qualitative consequences [34]. Indeed, we shall demonstrate that the topological order of the ground state of Eq. (1) is changed to the double-semion order. Such RVB-type wave functions with double-semion topological order could serve as candidate ground states of frustrated spin-1/2  $SU(2)$ -symmetric quantum magnets with frustrated Heisenberg interactions. Naively, Eq. (1) seems to be not invariant under the time reversal symmetry as  $it$  goes to  $-it$  under complex conjugate  $K$ . However, since the quantum dimer model can be viewed as the low-energy effective model in spin-singlet subspace, time-reversal symmetry can be realized in a much more generic form with  $T = UK$ , where  $UU^* = 1$  is a uni-

\* qiyang@tsinghua.edu.cn

† zgu@perimeterinstitute.ca

‡ yaohong@tsinghua.edu.cn

tary transformation (the detailed form of  $U$  will be discussed later). Actually, the time-reversal symmetry becomes manifested in the low-energy effective-field theory description for double-semion topological order, with

$$\mathcal{L} = \frac{K_{IJ}^{\text{DS}}}{4\pi} \epsilon^{\lambda\mu\nu} a_{I\lambda} \partial_\mu a_{J\nu}, \quad K_{IJ}^{\text{DS}} = \begin{pmatrix} 2 & 0 \\ 0 & -2 \end{pmatrix}. \quad (2)$$

In Sec. II, we construct the ground state wave function of Eq. (1). We show that under a proper local unitary transformation (which preserves the topological order), the ground state wave function takes an extremely simple form and can be described by an equal-weight superposition of all dimer configurations with signs of  $\pm 1$ , and the signs of different dimer configurations are determined by counting the number of loops in the corresponding transition graph.

In Sec. III, we explicitly demonstrate that the ground state we constructed has the double-semion topological order. In particular, the monomer excitations obey the fusion rules and statistics of the semion excitations. We first construct the sign structure of the monomer wave function using a string operator which we call a “half-vison string.” Using this result, the semionic statistics of monomers is illustrated using the procedure first proposed in Ref. 35, where the statistical phase of exchanging two monomers is determined by comparing the Berry phases of exchanging two monomers and moving one monomer along the same path.

Our construction of exactly solvable quantum dimer models with the double-semion topological order can be generalized to other two-dimensional nonbipartite lattices. In Sec. IV, we generalize our construction to the star lattice (which is also known by many other names summarized in Ref. 36) and to the kagome lattice. The star lattice is an interesting playground to study the quantum dimer models and spin-1/2 Kitaev models [37] as it has many nice properties [36], which are discussed in more detail in Sec. IV, and antiferromagnets on the star lattice have been realized in a polymetric iron acetate material [38]. On the star lattice, both the model Hamiltonian and its ground-state wave function are fully symmetric. Furthermore, we demonstrate the double-semion topological order of the ground-state wave function by mapping our model to the string-net model [21] and to a symmetry-protected topological (SPT) state in a spin model [39]. We also generalize our construction to the kagome lattice. Lastly, further discussions and the conclusion will be presented in Sec. V.

## II. SIGN STRUCTURES IN DIMER WAVE FUNCTION

We start with a brief review of the exactly solvable RK Hamiltonian and its ground-state wave function with the toric-code topological order. On the triangular lattice,

the RK Hamiltonian takes the following form [19]:

$$H_{\text{RK}} = \sum_{\text{plaquette}} -t (|\nearrow\rangle \langle \nwarrow| + \text{H.c.}) + v (|\nearrow\rangle \langle \nearrow| + |\nwarrow\rangle \langle \nwarrow|),$$

where the sum runs over all rhombic plaquettes. This Hamiltonian is exactly solvable at  $t = v$ , known as the RK point, because there the Hamiltonian can be rewritten as a sum of projection operators as follows,

$$H_{\text{RK}} = t \sum_{\text{plaquette}} (|\nearrow\rangle - |\nwarrow\rangle) ( \langle \nearrow| - \langle \nwarrow| ). \quad (3)$$

As a result, the wave function

$$|\Psi\rangle = \sum_c |c\rangle, \quad (4)$$

which is an equal-amplitude superposition of all dimer configurations, is an exact ground state of the Hamiltonian (here  $c$  denotes a dimer configuration). It can be shown that this wave function has the  $\mathbb{Z}_2$  topological order, which is the same as the toric-code model.

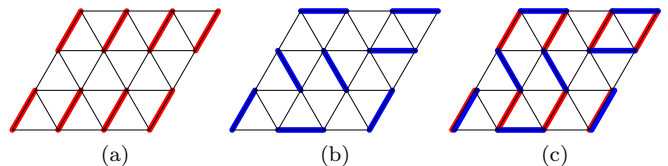


FIG. 1. Sign rule of dimer configurations. (a) The reference dimer configuration, which is a columnar VBS state. (b) An arbitrary dimer configuration. (c) The transition graph constructed by superposing the configurations in (a) and (b). In this transition graph, there are four loops, including two trivial length-two loops at the bottom-left and the bottom-right corners, and therefore the count  $N_c = 4$  in Eq. (6).

In this work, we construct a dimer wave function with the double-semion topological order. Motivated by the construction of wave functions with such topological order in the string-net models [21], we consider the following dimer wave function constructed as an equal-weight superposition of different dimer configurations with a sign structure:

$$|\Psi\rangle = \sum_c s(c) |c\rangle, \quad (5)$$

where  $s(c) = \pm 1$  is a sign function defined as follows. First, we construct a transition graph by superposing the dimer configuration  $c$  and a particular reference configuration  $c_0$ . Here we choose the reference  $c_0$  to be the columnar valence bond solid (VBS) configuration shown in Fig. 1(a). Then the sign function is determined from the number of transition loops  $N_c$  in the transition graph,

$$s(c) = (-1)^{N_c}. \quad (6)$$

Note that in the transition graph, if the two dimer configurations occupy the same bond, the two overlapping dimers form a trivial length-two loop. This trivial loop also contributes a factor of  $-1$  in the wave function. The construction of transition loops is demonstrated with an

example in Fig. 1(c).

Next, we show that the wave function in Eq. (5) is the exact ground state of the following extended RK Hamiltonian at the RK point  $t = v$ :

$$\begin{aligned} H_{\text{RK}}^{\text{ext}} = & \sum [t (|\nearrow\rangle \langle \nearrow| + \text{H.c.}) + v (|\nearrow\rangle \langle \nwarrow| + |\nwarrow\rangle \langle \nearrow|)] \\ & + \sum [(-1)^y t (|\nwarrow\rangle \langle \nwarrow| + \text{H.c.}) + v (|\nwarrow\rangle \langle \swarrow| + |\swarrow\rangle \langle \nwarrow|)] \\ & + \sum [t (|\leftrightarrow\rangle \langle \leftrightarrow| + \text{H.c.}) + v (|\leftrightarrow\rangle \langle \updownarrow| + |\updownarrow\rangle \langle \leftrightarrow|)], \end{aligned} \quad (7)$$

where the three sums run over rhombic resonance plaquettes in three different orientations respectively, and the sign of the resonance terms with the second orientation alternates in even and odd rows, as indicated by the factor of  $(-1)^y$  [ $y$  is the coordinate in the  $y$  direction, as labeled in Fig. 2(a)]. This Hamiltonian differs from the original RK Hamiltonian in Eq. (3) where the signs of the resonance term on some plaquettes become positive. For clarity, in the rest of the paper, we denote the plaquettes with positive and negative resonance terms in Eq. (7) as type-A and type-B plaquettes, respectively, as shown in Fig. 2(a).

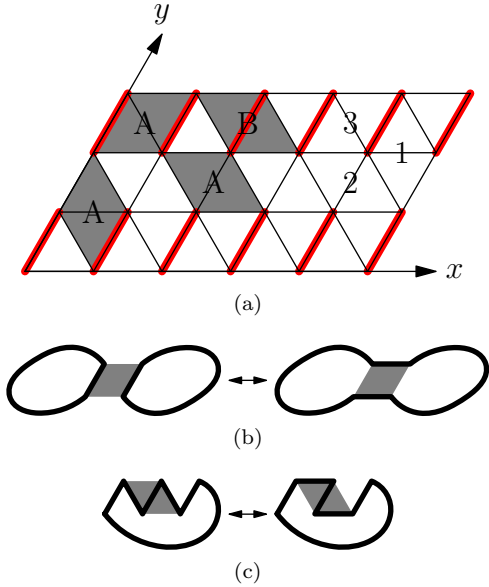


FIG. 2. Different types of resonance terms and their effects on transition graphs. The shaded rhombus shows the location of the resonance term, and the thick lines in (b) and (c) are transition loops. (a) Two types of resonance terms. The red dimers show the reference dimer configuration as in Fig. 1(a). (b) Effect of a type-A resonance term. A type-A term reconnects two transition loops and changes the number of loops by one. (c) Effect of a type-B resonance term. A type-B resonance term reconnects the loop locally and does not change the number of loops.

Similar to the original RK Hamiltonian, at the RK point  $t = v$  this extended RK Hamiltonian can also be written as a sum of projection operators on all plaquettes as follows,

$$\begin{aligned} H_{\text{RK}}^{\text{ext}} = & t \sum_A (|\nearrow\rangle + |\nwarrow\rangle) (\langle \nearrow| + \langle \nwarrow|) + \\ & t \sum_B (|\nwarrow\rangle - |\swarrow\rangle) (\langle \nwarrow| - \langle \swarrow|), \end{aligned} \quad (8)$$

where the two sums run over type-A and type-B plaquettes, respectively. Hence, similar to the original RK Hamiltonian, the ground state of this Hamiltonian is also a superposition of dimer configurations that are annihilated by all projection operators in Eq. (8). From the form of projection operators, we see that the ground-state wave function should be an equal-amplitude superposition of two different configurations resonating on a type-B plaquette, but an equal-weight superposition with opposite signs of two different configurations resonating on a type-A plaquette. We shall argue that the sign function defined in Eq. (6) by counting the number of transition loops satisfies these requirements. To see this, we first notice that a difference between type-A and type-B plaquettes is that in a type-B plaquette, the dimer at the middle of the plaquette belongs to the reference dimer configuration, while in a type-A plaquette it does not, as shown in Fig. 2(a). As a result, the two types of resonance terms act differently in the transition graphs, as shown in Fig. 2: A resonance term on a type-A plaquette reconnects two transition loops into one (or splits one into two), and therefore changes the parity of the total number of transition loops. On the other hand, a resonance term on a type-B plaquette alters a transition loop locally without changing the number of transition loops. As a result, the wave function defined using the sign in Eq. (6) is indeed a ground state of the extended RK Hamiltonian in Eq. (7) at  $v = t$ .

The global phase diagram of the extended RK Hamiltonian can be obtained by mapping it to the original RK Hamiltonian via a (nonlocal) unitary transformation that redefines the dimer basis using the sign function,

$$|c\rangle \rightarrow |\tilde{c}\rangle = s(c) |c\rangle. \quad (9)$$

After this (nonlocal) unitary transformation, the wave function in Eq. (5) becomes the original RK wave function in Eq. (4) and, using the previous argument one can show that the extended RK Hamiltonian in Eq. (7) becomes the original RK Hamiltonian in Eq. (3). Thus, we show that the wave function in Eq. (5) is an exact ground state of the extended RK Hamiltonian at  $v = t$ . Similar to the original RK Hamiltonian, the extended Hamiltonian we study also has a first-order phase transition at  $v = t$ , separating a staggered valence bond solid phase at  $v > t$  and a gapped liquid phase at  $v < t$ , which is smoothly connected to the exact wave function at  $v = t$  in Eq. (5). Hence, in this work, we use this wave function as a representative wave function to study the gapped liquid phase and the topological order therein. We also stress that the  $H_{\text{RK}}^{\text{ext}}$  and  $H_{\text{RK}}$  indeed have different topological orders since Eq. (9) is not a *local* unitary transformation.

Finally, we show that  $H_{\text{RK}}^{\text{ext}}$  and  $H$  have the same topological order since they can be mapped to each other through a *local* unitary transformation, defined by  $b_{ij} \rightarrow b_{ij}e^{i\theta_{ij}}$ , where the bosonic operator  $b_{ij}$  (with  $b_{ij}^2 = 0$ ) annihilates the dimer excitation on the bond  $(ij)$ , and  $\theta_{ij}$  is a phase factor that depends on the bond. As shown in Fig. 2(a), here we assign  $\theta_{ij} = 0$  for bonds with the first orientation,  $\theta_{ij} = \pi/4$  for bonds with the second orientation, and  $\theta_{ij} = \pi/4$  ( $3\pi/4$ ) for bonds with the third orientation on even (odd) rows, respectively. With this local unitary transformation, one can check that the Hamiltonian defined in Eq. (7) becomes the one we have introduced at the beginning of the paper in Eq. (1), and the wave function defined in Eq. (5) becomes

$$|\Psi_0\rangle = \sum_c (-1)^{N_c} e^{i\frac{\pi}{4}N_2} e^{i\frac{\pi}{4}N_3^{\text{even}}} e^{i\frac{3\pi}{4}N_3^{\text{odd}}} |c\rangle, \quad (10)$$

where  $N_2$  denotes the total number of dimers in the second orientation, and  $N_3^{\text{even}}$  ( $N_3^{\text{odd}}$ ) denotes the number of dimers in the third orientation on even (odd) rows, respectively. This local unitary transformation restores the translation and rotation symmetries in  $H$ . In addition, the ground-state wave function of  $H$  also preserves translation and rotation symmetries because, using the (nonlocal) unitary transformation in Eq. (9), we can show that  $|\Psi_0\rangle$  is the unique ground state (within a topological section) of the Hamiltonian, which itself is invariant under these symmetry transformations.

Since  $H_{\text{RK}}^{\text{ext}}$  is real and manifestly time-reversal invariant, the above local unitary transformation implies the time-reversal symmetry operator of  $H$  should be defined by  $T = UK$  with  $U : b_{ij} \rightarrow b_{ij}e^{i\theta_{ij}}$ , which is different from the physical time-reversal operation if the dimers are interpreted as spin-singlet pairs in a spin model. Therefore, in this context, the model in Eq. (1) breaks time-reversal symmetry (and also inversion symmetry). However, such an antiunitary operation may be realized as the physical time-reversal operation if the dimers are interpreted in other physical contexts.

On the other hand, we note that the Hamiltonian in Eq. (7) explicitly breaks symmetries of the trian-

gular lattice because the local unitary transformation  $e^{i\frac{\pi}{4}N_2} e^{i\frac{\pi}{4}N_3^{\text{even}}} e^{i\frac{3\pi}{4}N_3^{\text{odd}}}$  does not preserve these symmetries. In particular, it breaks the six-fold rotational symmetry and the translational symmetry along the  $y$  direction, as the resonance terms have different signs in different orientations and on different rows. The wave function defined in Eq. (5) also lacks these lattice symmetries, as its definition is based on a specific reference dimer configuration that breaks them. However, this is not essential to our study of the topological order in the state, as the intrinsic topological order we are interested in requires no symmetry to protect it.

In summary, in this section, we construct a wave function using a sign structure determined by the number of transition loops in the transition graph against a particular reference dimer configuration. This wave function is constructed as the ground state of an exactly solvable RK-like Hamiltonian, given by Eq. (1). We construct two forms for the exactly solvable Hamiltonian and its ground-state wave function, which are related by a local unitary transformation. The first form in Eqs. (7) and (5) breaks rotation and translation symmetries, while the second form in Eqs. (1) and (10) preserves all of the lattice symmetries but with twisted time-reversal and mirror symmetries. Despite the different symmetries, the two ground-state wave functions have the same intrinsic topological order, which does not need the protection of any global symmetry. Although  $H$  appears to be simpler,  $H_{\text{RK}}^{\text{ext}}$  has a simpler ground-state wave function. Hence, in Sec. III we use  $H_{\text{RK}}^{\text{ext}}$  to discuss the intrinsic topological order in the ground state.

### III. MONOMER EXCITATIONS AND THEIR STATISTICS

Now we study the topological order in the ground-state wave function introduced in the previous section by investigating the topological excitations above the ground state. In particular, we consider the monomer excitations, which are sites that have no dimer connected to them. In the dimer liquid state with the toric-code topological order, the monomer excitations are themselves bosons but have a nontrivial mutual statistics with another type of topological excitations called the visons. Here we shall show that for the dimer liquid state described by the wave function in Eq. (5), the monomer excitations obey nontrivial semionic statistics. The statistics of the topological excitations implies that the ground state features the so-called double-semion topological order instead of the toric-code order in the original RK wave function.

We begin with a brief review of the topological excitations in the double-semion topological order. In such a state, there are three types of excitations: the semion, the antisemion and the bosonic bound state of two semions. The statistics and fusion rules of these excitations are summarized in Tables I and II, respectively. We shall see

TABLE I. Self- and mutual statistics of topological excitations in the double-semion topological order.  $s$ ,  $\bar{s}$ , and  $b$  denotes the semion, the antiseimion and the bosonic bound state, respectively.

$e^{i\theta}$	$s$	$\bar{s}$	$b$
$s$	$i$	0	-1
$\bar{s}$	0	$-i$	-1
$b$	-1	-1	0

TABLE II. Fusion rules between topological excitations in the double-semion topological order.

$\times$	$s$	$\bar{s}$	$b$
$s$	1	$b$	$\bar{s}$
$\bar{s}$	$b$	1	$s$
$b$	$\bar{s}$	$s$	1

that in the extended quantum dimer models, these three types of excitations correspond to two types of monomers and the vison, respectively.

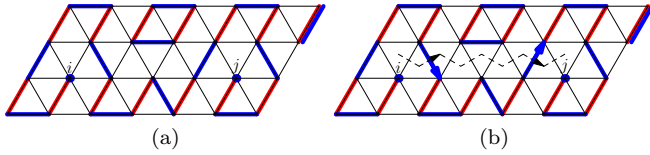


FIG. 3. A monomer string and a half-vison string. (a) The transition graph of a dimer configuration with two monomer excitations. Besides the transition loops, the graph also contains a string connecting two monomer sites, for which we coin the name “monomer string.” (b) A half-vison string connecting the two monomer sites. The half-vison string is represented by a dashed line. Both the monomer string and the half-vison string are oriented from site  $i$  to  $j$ . The arrows on the dimers and the dashed line show the direction of monomer and half-vison strings. Note that the half-vison string runs through the dual lattice, so it starts and ends on an adjacent dual lattice site to the monomer excitations. According to the definition of the half-vison string, the two crossings at the left and the right gives phase factors of  $-i$  and  $i$ , respectively. This is explained in Appendix B.

First, we consider the dimer wave function that contains monomer excitations at fixed locations. The monomer wave function is an eigenstate of the Hamiltonian in Eq. (7) in the Hilbert space that consists of dimer configurations that have no dimer connecting to the monomer sites. We start with the simple case that has two monomers at sites  $i$  and  $j$ , and consider a wave function that is a superposition of different dimer configurations,

$$|\Psi(i, j)\rangle = \sum_{c[i, j]} s(c[i, j]) |c[i, j]\rangle, \quad (11)$$

where  $c[i, j]$  denotes dimer configurations with two

monomer defects at sites  $i$  and  $j$ . To determine the phase factor  $s(c[i, j])$ , we again consider the transition graph between the configuration  $c[i, j]$  and the reference state in Fig. 1(a). Since the configuration  $c[i, j]$  has two monomer defects, besides the transition loops the transition graph also contains a string connecting the two defect sites  $i$  and  $j$ , as illustrated with an example in Fig. 3(a). In this paper, we coin the name “monomer string” for this string. Hence naturally in the phase factor  $s(c[i, j])$ , besides the factor of  $-1$  contributed from each transition loop, there is an extra phase factor depending on the configuration of the monomer string,

$$s(c[i, j]) = (-1)^{N_c} \phi(M_{ij}), \quad (12)$$

where  $M_{ij}$  denotes the monomer string connecting  $i$  and  $j$ .

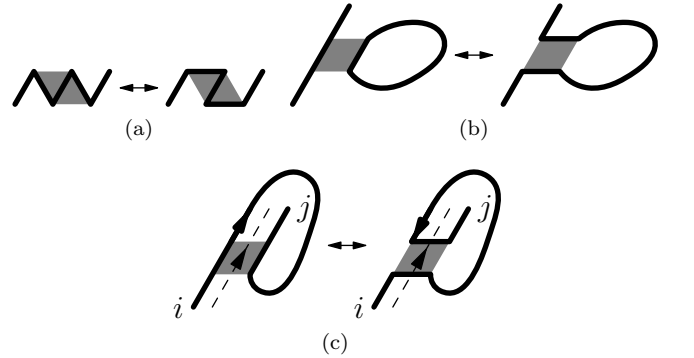


FIG. 4. Effects of different types of resonance terms on the defect string connecting two monomers. Similar to Fig. 2, the shaded area shows the location of the resonance term and the thick line shows the defect string that connects two monomer excitations. The dashed line shows the half-vison string. (a) A type-B resonance term changes the shape of the string locally without changing the topology of the string. (b) A type-A resonance term absorbs a nearby loop into the string. (c) A type-A resonance term reconnects the monomer string. In the left configuration the half-vison string does not intersect the monomer string, and in the right configuration the half-vison string intersects the monomer string twice with the same phase factors  $i$ , so the total phase is  $-1$ . Therefore, the half-vison string gives an extra phase factor  $-1$  after the resonance.

To determine the form of  $\phi$ , we study how the resonance terms in the extended RK Hamiltonian act on the monomer string. The type-B terms act trivially on the monomer string by changing the shape of the string locally, as shown in Fig. 4(a), while it does not change the sign of the wave function. The type-A terms, on the other hand, act in two ways on the monomer string. First, in Fig. 4(b), the action of such resonance term merges the string with a nearby loop. In this process the wave function changes sign because the type-A term is positive in the Hamiltonian, while the count of loop number  $N_c$  also changes by one. Therefore, the factor  $\phi(M_{ij})$  is unchanged in this resonance process. Second,

in Fig. 4(c), it is illustrated that after the action of a type-A resonance term, the string is reconnected with itself and no transition loop is created or annihilated. Since the type-A term is positive in the Hamiltonian, and  $N_c$  stays the same, the phase factor  $\phi(M_{ij})$  must acquire a minus sign. Such a phase factor can be constructed using another string operator connecting the two monomer sites through the dual lattice. This string operator acts like a square root of the vison string operator; therefore, we coin the name “half-vison string.”

The definition of a half-vison string operator is illustrated in Fig. 3(b). Here we only give a simplified version of its definition for the special case that there are only two monomers and the half-vison string connects the two monomer sites. (Since the half-vison string goes through the dual lattice, when we say the half-vison string connects a monomer site we mean the string terminates at a nearest-neighbor dual lattice site around the monomer site. In Appendix B, we discuss this in more detail and show that this arbitrary choice does not affect our result.) The definition for general cases is given in Appendix B. We first assign a direction to the monomer string in the transition graph, and the half-vison string is also oriented. The action of the string operator is then defined as a product of phase factors everytime the half-vison string and the monomer string intersect. The phase factor at the intersection point depends on the angle between the dimer and the half-vison string: the phase factor is  $i$  if the dimer runs from the right to the left relative to the direction of the half-vison string, and  $-i$  otherwise. Some basic properties of the half-vison string operator are discussed in Appendix B: Similar to the vison string operator, it is also independent of the choice of the path and effectively defines two local operators at the two ends of the string. Moreover, two parallel half-vison strings fuse into one vison string, which is the reason we chose its name.

The phase factor  $\phi(M_{ij})$  in the two-monomer wave function can be chosen to be the phase factor of a half-vison string operator that connects the two monomers,

$$\phi(M_{ij}) = H_{i \rightarrow j}(M_{i \rightarrow j}), \quad (13)$$

where  $H_{i \rightarrow j}$  denotes a half-vison string operator from  $i$  to  $j$ , and  $M_{i \rightarrow j}$  denotes the oriented monomer string. To prove that the wave function constructed with this phase factor is indeed an eigenstate of the Hamiltonian in Eq. (7), we need to show that the phase factor in Eq. (13) is invariant under the resonance processes shown in Figs. 4(a) and 4(b), but changes sign in Fig. 4(c). Since the half-vison string operator is path independent, we can choose its path to simplify our discussion. For the resonance processes in Figs. 4(a) and 4(b), we choose the path of the half-vison string such that it does not intersect with the piece of monomer string shown in the figures. Therefore, the phase factor in Eq. (13) is indeed unchanged. For the resonance process in Fig. 4(c), we let the half-vison string cut through the resonance pla-

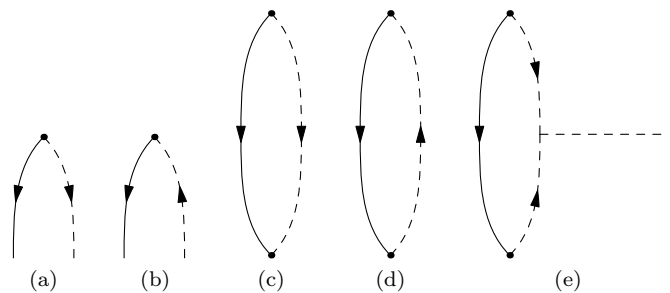


FIG. 5. Monomer excitations and fusion rules. The solid lines with arrows are the monomer strings, and dashed lines with arrows are the half-vison strings. The dashed line without an arrow is a vison string. (a) A monomer excitation with one outgoing monomer string and one outgoing half-vison string. (b) An antimonomer with one outgoing monomer string and one incoming half-vison string. (c) Two monomers are joined by one monomer string and one half-vison string running in parallel directions and fuse into vacuum. (d) Two antimonomers are joined by one monomer string and one half-vison string running in opposite directions and fuse into vacuum. (e) One monomer and one antimonomer are joined by one monomer string, but the two half-vison strings meet in the middle and fuse into a vison string. Hence one monomer and one anti-monomer fuse into a vison.

quette, as shown in that figure. It is easy to check that after the resonance, the phase factor  $\phi(M_{ij})$  acquires a minus sign, which is consistent with the Hamiltonian. Therefore, the two-monomer wave function defined using  $\phi(M_{ij})$  in Eq. (13) is indeed an eigenstate of the Hamiltonian in Eq. (7).

Similarly, one can construct another wave function using a half-vison string running in the opposite direction,

$$\phi^*(M_{ij}) = H_{j \rightarrow i}(M_{i \rightarrow j}), \quad (14)$$

and using the definition of half-vison string it is easy to see that this phase factor is the complex conjugate of the one in Eq. (13). In this construction, the monomer excitations can be viewed as a bound state of one end of a monomer string and one end of a half-vison string. Because both types of strings are oriented, the monomer belongs to different types depending on the direction of the strings. Since the wave function is invariant if both the monomer string and the half-vison string are reversed, there are two types of monomer excitations, with the two strings in the same or opposite directions, respectively. We denote the bound state of two starting or two ending points of the two strings as the monomer, and the bound state of one starting and one ending point of the two strings as the antimonomer, respectively, as illustrated in Figs. 5(a) and 5(b). Using this convention, the wave function  $|\Psi(i, j)\rangle$  contains two monomer excitations, whereas its complex conjugate  $|\Psi^*(i, j)\rangle$  contains two antimonomers.

In the two-monomer Hilbert space, there are two degenerate ground-state wave functions  $|\Psi(i, j)\rangle$  and



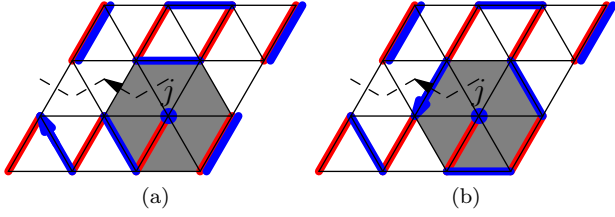


FIG. 6. Length-six resonance term.

$|\Psi^*(i, j)\rangle$ , representing states with two monomers or two antimonomers, respectively. This double degeneracy of two-monomer states is accidental and not protected by the topological order. In particular, it can be lifted by local perturbations near the monomer excitations [40]. As an example, we consider a resonance term on a length-six loop surrounding one monomer excitation, as shown in Fig. 6. For the configuration shown in this example, the action of the resonance term annihilates one transition loop and creates one intersection between the half-vison string and the monomer string with the factor  $i$ . Hence the sign of the two-monomer wave function  $|\Psi(i, j)\rangle$  changes by  $-i$ . On the other hand, the two-antimonomer wave function  $|\Psi^*(i, j)\rangle$  changes by  $i$ . Therefore, adding such a resonance term with coefficient  $\mp i$  to the Hamiltonian lifts the degeneracy and favors the state with two monomers and two antimonomers, respectively, as this term breaks the time-reversal symmetry which relates the two wave functions  $|\Psi(i, j)\rangle$  and  $|\Psi^*(i, j)\rangle$ .

Using the construction of the wave function, we can check the fusion rules between monomer, antimonomer, and vison excitations, as illustrated in Fig. 5. First, if we have two monomers, they can be joined by one monomer string and one half-vison string running in the same direction, and therefore they fuse into a trivial state. Likewise, two antimonomers can be joined by one monomer string and one half-vison string running in opposite directions, and also fuse into a trivial state. On the other hand, if we have one monomer and one antimonomer, they can be joined by one monomer string, but there are two half-vison strings coming out from them. The two half-vison strings meet and they can fuse into one vison string (see Appendix B). Therefore, one monomer and one antimonomer fuse into a vison.

Next, we explicitly demonstrate the nontrivial semionic statistics of monomer excitations by calculating the exchange algebra between two monomer excitations. This can be computed by first calculating the Berry phase acquired by exchanging two monomers, then subtracting the Berry phase acquired by moving one monomer along the same path [35].

As a demonstration, we consider the exchange process on the dimer configurations shown in Fig. 7 and corresponding hopping process shown in Fig. 8. The Berry phase accumulated through the exchange process is determined by multiplying the signs of the hopping and res-

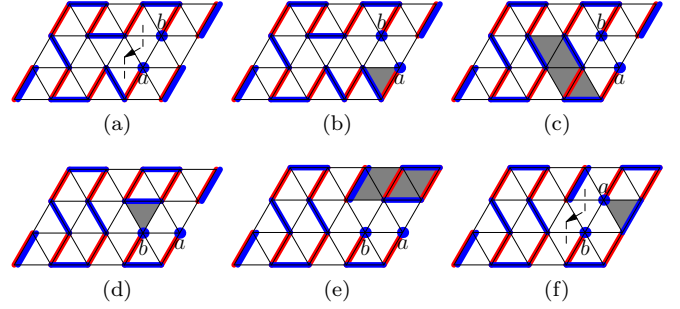


FIG. 7. Exchanging two monomers.

onance terms used in the process, and the relative phase between the initial and final dimer configurations. In the exchange process, we used three hopping terms, which exchange the location of the monomer with a nearby dimer in the shaded triangle. Here the signs of the hopping terms can be neglected, because the same hopping terms are also used in Fig. 8 and the signs will cancel when subtracting the two Berry phases. From the Hamiltonian in Eq. (7), we see that the product of the signs of the resonance terms used in Fig. 7 is  $+1$ . The relative phase between the initial and final dimer configurations in Figs. 7(a) and 7(b) is  $-1$ , since one transition loop is created during the process, and the half-vison string contributes no factor in both Figs. 7(a) and 7(f). Therefore, the total Berry phase acquired in Fig. 7 is  $-1$ . The Berry phase acquired in the hopping process in Fig. 8 can be determined similarly. Here the total sign of the resonance terms is again  $+1$ , and according to the sign of the monomer wave function defined in Eq. (11), the relative sign between the final state in Fig. 8(e) and the initial state in Fig. 8(a) is  $i$ , as the parity of the number of loops is the same, but the half-vison string cuts the monomer string once with a phase factor  $i$  in Fig. 8(e). Therefore, the total Berry phase is  $i$ . Subtracting this from the Berry phase in Fig. 7, we conclude that the statistical phase accumulated by exchanging two monomers is  $i$ , which is consistent with exchanging two semions as listed in Table I.

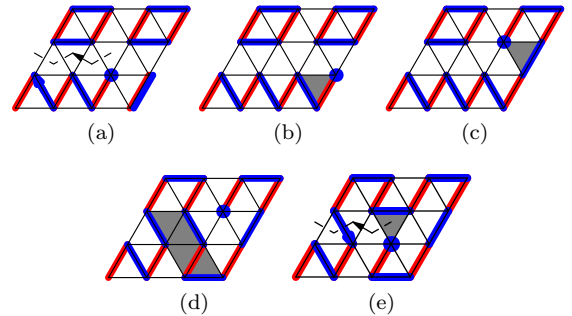


FIG. 8. Moving one monomer along exactly the same path as in Fig. 7.

Similarly, if we were exchanging two antimonomers instead, the statistical phase determined by the previous argument would become  $-i$  because the winding angle in Fig. 8(a) becomes  $-2\pi$  as the monomer string reverses its direction. Therefore, we conclude that the monomer and antimonomer excitations obey the statistics and fusion rules of semion and antiseimion excitations in the double-semion topological order, respectively. This implies that the gapped phase represented by the wave function in Eq. (5) indeed has the double-semion topological order.

#### IV. GENERALIZATION TO THE STAR LATTICE

Our construction of the dimer wave function with the double-semion topological order and the corresponding exactly solvable Hamiltonian can be easily generalized to other two-dimensional nonbipartite lattices, such as the star lattice and the kagome lattice. In particular, when generalized to the star lattice, the constructed wave function and the corresponding exactly solvable quantum dimer Hamiltonian are invariant under both time-reversal and lattice symmetries in an obvious way. We also briefly discuss the generalization to the kagome lattice.

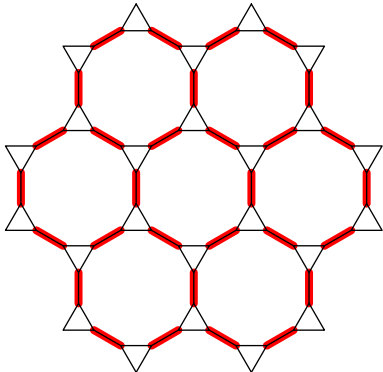


FIG. 9. Fully symmetric dimer configuration on the star lattice.

The dimer wave function constructed in Eq. (5) for the triangular lattice breaks lattice symmetries because the choice of the reference dimer configuration breaks them. However, on the star lattice, a fully symmetric dimer configuration exists, as shown in Fig. 9. Using this configuration as the reference, the wave function constructed in Eq. (5) becomes fully symmetric.

Furthermore, an exactly solvable Hamiltonian can be constructed such that the wave function in Eq. (5) is its ground state. Similar to the kagome lattice, on the star lattice the dimer configurations also have arrow and pseudospin representations [36, 41, 42], and from these representations an exactly solvable Hamiltonian whose ground state is the RK wave function is constructed as

follows [36, 42]:

$$H = - \sum_D \sum_{\alpha} [ |L_{\alpha}(D)\rangle \langle \bar{L}_{\alpha}(D)| + \text{H.c.} ], \quad (15)$$

where the sum runs over all dodecagons labeled by  $D$ , and on each dodecagon the sum runs over all even-length resonance loops surrounding it. For each dodecagon, there are 32 such loops, denoted by  $\alpha = 1, \dots, 32$ . For each loop  $\alpha$  on the dodecagon  $D$ ,  $L_{\alpha}$  and  $\bar{L}_{\alpha}$  denote the two different dimer configurations that form the resonance loop. It is shown in Ref. 36 that the ground state of this Hamiltonian is the RK wave function in Eq. (4) which supports  $Z_2$  topological order. To obtain the Hamiltonian for the double-semion wave function in Eq. (5), we use the unitary transformation in Eq. (9). After this unitary transformation, the RK wave function in Eq. (4) is mapped to the double-semion wave function in Eq. (5), and the Hamiltonian in Eq. (15) is mapped to the following form:

$$H = - \sum_D \sum_{\alpha} \left[ (-1)^{\frac{l(\alpha)}{2}+1} |L_{\alpha}(D)\rangle \langle \bar{L}_{\alpha}(D)| + \text{H.c.} \right], \quad (16)$$

where  $l(\alpha)$  denotes the length of the resonance loop (which is always even).

The double-semion topological order in the ground state of the Hamiltonian in Eq. (16) can be understood by repeating the argument in Sec. III on the star lattice. Moreover, it can also be shown using dualities to two previously studied models with the double-semion topological order. First, this dimer model on the star lattice can be mapped to a loop model, which is a special case of the general string-net models discussed in Ref. 21. Because the star lattice is trivalent (each lattice site has three nearest neighbors), a dimer configuration on such a lattice can be mapped to a loop configuration [43], which occupies the bonds that are not occupied by the dimers. Under this mapping, the original RK wave function is mapped to an equal-amplitude superposition of all loop configurations, which carries the toric-code topological order [21]. On the other hand, the wave function in Eq. (5) is mapped to an equal-weight superposition of loop configurations with a sign structure. Using the Hamiltonian in Eq. (16), we can show that the ground-state wave function in the loop model has the following form:

$$|\Psi\rangle = \sum_X (-1)^{X_c} |X\rangle, \quad (17)$$

where  $X$  denotes all possible loop configurations, and  $X_c$  is the count of loops in a configuration. As shown in Ref. 21, this wave function has the double-semion topological order. This implies that the corresponding dimer wave function also has this nontrivial topological order.

Second, the quantum dimer model in Eq. (16) can be mapped to a symmetry-protected topological (SPT) state discussed in Ref. 39. Using the pseudospin representation, quantum dimer models on the star lattices can be



mapped to a spin model [36] with pseudospin degrees of freedom that locate at the centers of the dodecagon and form a triangular lattice. In this mapping, the domain walls in the spin configuration correspond to the loops in the transition graph against an arbitrary reference dimer configuration (in our case, the reference configuration can be chosen as the state in Fig. 9). The model in Eq. (15) is mapped to the following spin model:

$$H = -\Gamma \sum_D \sigma^x(D), \quad (18)$$

where  $\sigma^x(D)$  is the Pauli matrix operator that acts on the pseudospin. The ground state of this pseudospin Hamiltonian is a trivial paramagnetic state. If we map this pseudospin model back to a quantum dimer model, the mapping between the pseudospin and dimer states is two to one, where two spin configurations related by the operation  $\prod_D \sigma^x(D)$  are mapped to the same dimer configuration. Therefore, the operation  $\prod_D \sigma^x(D)$  is a  $Z_2$  global symmetry in the pseudospin model and becomes a gauge symmetry in the quantum dimer model. In Ref. 39, it is shown that gauging a  $Z_2$  symmetry in a trivial paramagnetic state gives a state with the toric-code topological order, which is consistent with the intrinsic topological order carried by the original RK wave function. Next, we consider mapping the quantum dimer model in Eq. (16) to a spin model in the pseudospin representation. Since the loops in the transition graph are mapped to domain walls in the pseudospin configuration, the total number of loops  $N_c$  in the sign structure of the wave function in Eq. (5) is mapped to the total number of domain walls. Therefore, the ground-state wave function in Eq. (5) is mapped to the spin wave function discussed in Ref. 39,

$$|\Psi\rangle = \sum_{\{\sigma_D^z\}} (-1)^{N_{\text{dw}}} |\{\sigma_D^z\}\rangle, \quad (19)$$

where  $|\{\sigma_D^z\}\rangle$  denotes an Ising basis, and  $N_{\text{dw}}$  counts the number of domain walls in the spin configuration. Correspondingly, the Hamiltonian in Eq. (16) is mapped to the following form [39]:

$$H = -\Gamma \sum_D B_D, \quad B_D = -\sigma_D^x \prod_{\langle DD_1 D_2 \rangle} i^{\frac{1-\sigma_{D_1}^z \sigma_{D_2}^z}{2}}, \quad (20)$$

where the product in the definition of  $B_D$  runs over the six triangles  $\langle DD_1 D_2 \rangle$  containing the site  $D$ . In Ref. 39, it is shown that the ground state in Eq. (19) has a non-trivial SPT order, protected by the aforementioned global  $Z_2$  symmetry. Furthermore, gauging this  $Z_2$  symmetry gives a state with the double-semion topological order. This is consistent with our conclusion that the dimer state in Eq. (5) carries the double-semion topological order.

Similarly, this construction can be implemented on the kagome lattice, where the  $Z_2$  RK wave function is the ground state of an exactly solvable Hamiltonian [42] anal-

ogous to Eq. (15),

$$H = - \sum_H \sum_\alpha [ |L_\alpha(H)\rangle \langle \bar{L}_\alpha(H) + \text{h. c.} ], \quad (21)$$

where  $H$  iterates over all hexagons in the kagome lattice, and  $\alpha$  labels the even-length resonance loops surrounding a hexagon. On a kagome lattice, the double-semion dimer wave function in Eq. (5) can be constructed using a particular reference dimer configuration. Unlike the star lattice, such reference configuration always breaks translational symmetries of the kagome lattice, and as a result the constructed wave function and the corresponding exactly solvable Hamiltonian also lacks lattice symmetries. Again using the unitary transformation in Eq. (9) we can obtain the general form of the exactly solvable Hamiltonian whose ground state is the double-semion dimer wave function,

$$H = - \sum_{H,\alpha} \left[ (-1)^{\frac{l(\alpha)}{2} + r(H,\alpha) + 1} |L_\alpha(H)\rangle \langle \bar{L}_\alpha(H)| + \text{H.c.} \right], \quad (22)$$

where  $r(H,\alpha)$  counts the number of reference dimers which connect next-nearest-neighbor sites in the resonance loop  $\alpha$  around the hexagon  $H$ . We note that this Hamiltonian explicitly breaks lattice symmetries because of the factor  $r(H,\alpha)$ , which depends on the choice of the reference dimer configuration.

## V. DISCUSSION AND CONCLUSION

In this work, we study an exactly solvable model on the triangular lattice with a gapped spin-liquid ground state that has the double-semion topological order. Comparing to the original RK Hamiltonian, this exactly solvable Hamiltonian contains the same local resonance and potential terms, but the coefficient of the resonance term becomes imaginary. As a result, the ground-state wave function of this exactly solvable Hamiltonian has a nonlocal sign structure determined by counting the number of loops in the transition graph. Moreover, the wave function of monomer excitations also has a sign structure that can be constructed using a half-vison string. Using the sign structure in the ground state and the excited states, we explicitly demonstrate that the monomer excitations obey the fusion rules and the statistics of semion and antiseimion excitations. This implies that the ground state has the double-semion topological order.

We constructed two forms of an exactly solvable Hamiltonian realizing the same double-semion topological order, which are related by a local unitary transformation. In one form, it explicitly breaks translational and rotational symmetries of the lattice. The other form retains the lattice symmetries but realizes time-reversal and mirror symmetries in a twisted way. Furthermore, we also constructed a simple fully symmetric exactly solvable Hamiltonian on the star lattice.

Our construction of dimer wave functions with double-semion topological order can be generalized to construct spin wave functions in order to study spin-liquid states. (We note that a spin wave function with the double-semion topological order has been realized in a spin-1 system using a different approach [44].) For antiferromagnetic spin-liquid states with a large spin gap, a spin wave function analogous to the dimer wave function in Eq. (4) can be constructed as a superposition of different short-range spin-singlet pairing patterns [45, 46]. On a nonbipartite lattice, such wave functions have the  $Z_2$  topological order and a short-range spin-spin correlation [47, 48]. The properties of such wave functions can be studied numerically using the variational Monte Carlo [47, 48] and projected entangled pair states (PEPS) [49, 50] methods. A sign structure similar to the one used in the dimer wave function in Eq. (5) can be added to this spin-liquid wave function and this additional sign structure will change the topological order of the spin-liquid state to the double-semion one. In particular, on kagome lattices, recent numerical studies [28–31] reveal possible evidences of continuous phase transitions between the gapped spin-liquid ground state of the nearest-neighbor Heisenberg model and a time-reversal-symmetry-breaking chiral spin-liquid state, and it has been proposed theoretically [32] that such transitions imply that the former spin liquid has the double-semion topological order. Such a proposal can be investigated using the spin wave function we just proposed, and we shall leave this interesting work to future studies. (We note that since the double-semion topological order necessarily breaks time-reversal or lattice symmetries [51], such a proposal implies that the gapped spin-liquid ground state of the nearest-neighbor Heisenberg model breaks time-reversal or lattice symmetries. This symmetry breaking is not observed numerically and this issue needs to be resolved by future DMRG studies.)

*Note added.* After the completion of our work, we learned that the realization of double-semion topological order on kagome lattice quantum dimer models is also being considered by other works [52, 53].

## ACKNOWLEDGMENTS

We thank Liang Fu, Steve Kivelson, Chong Wang and Xiao-Gang Wen for invaluable discussions. Y.Q. is supported by NSFC Grant No. 11104154. Z.-C. G. is supported by is supported by the Government of Canada through Industry Canada and by the Province of Ontario through the Ministry of Research and Innovation. H.Y. is supported in part by the National Thousand-Young-Talent Program.

## Appendix A: Symmetry of the double-semion ground state

In this appendix, we argue that the double-semion ground-state wave function in Eq. (10) is invariant under the translation and rotation symmetries of the triangular lattice.

Both the exactly solvable Hamiltonian in Eq. (7) and its ground-state wave function in Eq. (5) break the translation and rotation symmetries of the triangular lattice because they depend on the choice of a symmetry-breaking reference state, as explained in Sec. II. However, the translation and rotation symmetries are restored in the Hamiltonian in Eq. (1) after the local unitary transformation  $b_{ij} \rightarrow b_{ij}e^{i\theta_{ij}}$ . After this local transformation, the ground-state wave function takes the form in Eq. (10). Here we prove that this wave function is invariant under lattice translation and rotations, although the form of Eq. (10) does not manifest these symmetries explicitly.

To show this, consider that the exactly solvable Hamiltonian in Eq. (1) is related to the original RK Hamiltonian by the combination of the global unitary transformation in Eq. (9) and the aforementioned local unitary transformation. Therefore, the two Hamiltonians have exactly the same spectrum. That is, all eigenstates of the two Hamiltonians (including the ground state and excited states) have the same energies and degeneracies, and the wave functions are related by the combined unitary transformation. Now we consider the ground states of the Hamiltonian. It is well known that for the original RK Hamiltonian, if we neglect the non-flippable states, which are disconnected with the rest of the states in the Hilbert space, then there are four ground states, one in each topological section labeled by the two winding numbers in the  $x$  and  $y$  directions. Hence there is a unique nondegenerate ground state in each topological sector. Because of the unitary transformation, the same claim also holds for the Hamiltonian in Eq. (1). Since the Hamiltonian is itself translational and rotational invariant, after these symmetry transformations the ground-state wave function must stay invariant, up to a global phase factor.

Another way of arguing this is that since the Hamiltonian in Eq. (7) respects translation and rotation symmetries, the ground-state wave function can only break these symmetries through spontaneous symmetry breaking, which would imply ground-state degeneracy in the spectrum of the Hamiltonian. However, neither the spectrum of this Hamiltonian nor that of the original RK Hamiltonian have the ground-state degeneracy corresponding to the spontaneous symmetry breaking. Note that the ground-state degeneracy due to spontaneous symmetry breaking is not to be confused with the topological ground-state degeneracy: the former degeneracy is between states within the same topological sector defined by the winding numbers, and the latter is between states in different topological sectors.

## Appendix B: Half-vison string operator

In this appendix, we discuss the definition and properties of the string operators we use in Sec. III to describe the sign structure of monomer wave functions. This string operator is used to define the semion and antisemion excitations, and it acts like the square root of a vison string. Therefore, we coin the name “half-vison string.” In Sec. III, the half-vison string operator is defined for the special cases that contain only two monomers and the half-vison string operator connects these two monomer sites. Here we give the definition for general cases and argue that this definition reduces to the simplified version in the special cases.

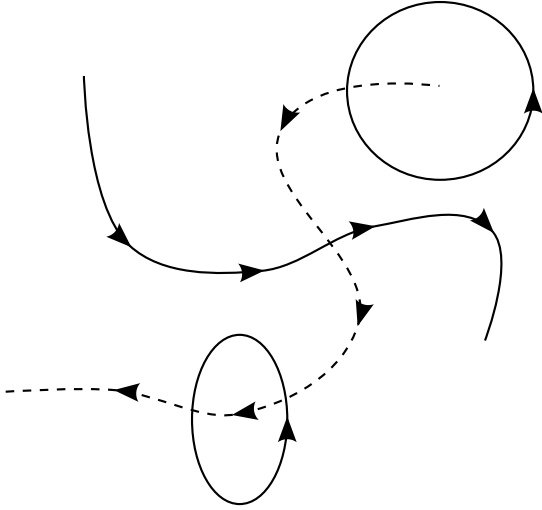


FIG. 10. General definition of a half-vison string operator. The solid lines represent loops and monomer strings in the transition graph, and the dashed line represents a half-vison string.

The general definition of the half-vison string operator is illustrated in Fig. 10. For any dimer configuration, we construct the transition graph between it and the reference configuration. In the transition graph, we assign orientations to both the monomer strings and transition loops. In Sec. III, we see that the orientation of a monomer string determines the type of monomers at its ends. For the transition loops, we always choose the orientation to be counterclockwise. Then the result of the half-vison string operator is the product of phase factors every time the half-vison string cuts a dimer, and the phase factor depends on the angles between the half-vison string and the dimer: the phase factor is  $i$  if the dimer is going from the left to the right relative to the direction of the half-vison string, and the phase factor is

$-i$  otherwise. From the definition of the semion string operator, we can deduce the following properties.

First, two semion string operators in the same direction becomes a vison string, as the square of the phase factors  $\pm i$  is always  $-1$ . Hence a semion string can be viewed as the square root of a vison string. We note that here we define a vison string as a string operator that contributes a  $-1$  sign every time it cuts a dimer in the transition graph, where dimers from the reference configuration are also counted. However, in most literature, it is defined without counting the dimer in the reference state. Since the dimer configuration in the reference state is fixed, the two definitions only differ by an overall factor that does not depend on the dimer configuration we consider.

Second, for dimer configurations with monomers at fixed locations, the semion string operator depends only on the starting and ending of the string and does not depend on the path. The difference between two different semion strings starting and ending at the same locations is a closed semion string loop. If such loop encloses no monomer sites, the loop intersects any transition loop or string even times and the phase factors cancel, so the closed string operator is equal to the identity operator, and therefore the two semion string operators are equal. Moreover, one can show that if the semion string loop encloses monomer excitations, the string loop operator is equal to a constant phase factor, which is a product from each enclosed monomer excitation, where a monomer with an outgoing and incoming transition string contributes a  $\pm i$ , respectively. Therefore, in this case, the two semion operators only differ by an overall phase factor.

Lastly, the general definition of a half-vison string can be reduced to the simplified form we use in Sec. III, where only intersections with the monomer string are considered, if there are only two monomers and the half-vison string connects the two monomer sites. Since the transition loops and the monomer strings do not intersect, in this case there is no transition loop that encloses any end of the half-vison string. Therefore, for every transition loop that the half vison cuts, it cuts it even times and the total phase factor cancels. Therefore, in this case only cuts, with the monomer string needs to be considered. We note that when we say the half-vison string starts or ends on a lattice site, there is an ambiguity on the exact location of the starting or ending point because the half-vison string lives on the dual lattice, and its starting (or ending) point can only be on a dual lattice. Here one dual lattice point around the monomer site can be arbitrarily chosen as the starting point of the half-vison string. Since in the transition graph there is only one dimer from the reference configuration connecting to the monomer site, and the position of this reference dimer is therefore fixed, this arbitrary choice of half-vison string starting (or ending) point does not affect the definition of the half-vison string operator up to an overall phase factor that does not depend on the dimer configuration.

- 
- [1] S. A. Kivelson, D. S. Rokhsar, and J. P. Sethna, Phys. Rev. B **35**, 8865 (1987).
  - [2] X.-G. Wen, Phys. Rev. B **40**, 7387 (1989).
  - [3] X.-G. Wen, Int. J. Mod. Phys. B **05**, 1641 (1991).
  - [4] M. Levin and X.-G. Wen, Phys. Rev. Lett. **96**, 110405 (2006).
  - [5] A. Kitaev and J. Preskill, Phys. Rev. Lett. **96**, 110404 (2006).
  - [6] X. Chen, Z.-C. Gu, and X.-G. Wen, Phys. Rev. B **82**, 155138 (2010).
  - [7] A. Y. Kitaev, Ann. Phys. (N. Y.) **303**, 2 (2003).
  - [8] C. Nayak, A. Stern, M. Freedman, and S. Das Sarma, Rev. Mod. Phys. **80**, 1083 (2008).
  - [9] D. C. Tsui, H. L. Stormer, and A. C. Gossard, Phys. Rev. Lett. **48**, 1559 (1982).
  - [10] R. B. Laughlin, Phys. Rev. Lett. **50**, 1395 (1983).
  - [11] X. G. Wen, F. Wilczek, and A. Zee, Phys. Rev. B **39**, 11413 (1989).
  - [12] X. G. Wen, Phys. Rev. B **44**, 2664 (1991).
  - [13] X.-G. Wen, Phys. Rev. Lett. **90**, 016803 (2003).
  - [14] P. W. Anderson, Science **235**, 1196 (1987).
  - [15] T. Senthil and M. P. A. Fisher, Phys. Rev. B **62**, 7850 (2000).
  - [16] P. Lee, N. Nagaosa, and X.-G. Wen, Rev. Mod. Phys. **78**, 17 (2006).
  - [17] D. S. Rokhsar and S. A. Kivelson, Phys. Rev. Lett. **61**, 2376 (1988).
  - [18] P. W. Anderson, Mater. Res. Bull. **8**, 153 (1973).
  - [19] R. Moessner and S. L. Sondhi, Phys. Rev. Lett. **86**, 1881 (2001).
  - [20] N. Read and S. Sachdev, Phys. Rev. Lett. **66**, 1773 (1991).
  - [21] M. A. Levin and X.-G. Wen, Phys. Rev. B **71**, 045110 (2005).
  - [22] A. Kitaev, Ann. Phys. (N. Y.) **321**, 2 (2006).
  - [23] S. Yan, D. A. Huse, and S. R. White, Science **332**, 1173 (2011).
  - [24] S. Depenbrock, I. P. McCulloch, and U. Schollwöck, Phys. Rev. Lett. **109**, 067201 (2012).
  - [25] H.-C. Jiang, Z. Wang, and L. Balents, Nat. Phys. **8**, 902 (2012).
  - [26] R. Suttner, C. Platt, J. Reuther, and R. Thomale, Phys. Rev. B **89**, 020408(R) (2014).
  - [27] M. Yamashita, N. Nakata, Y. Kasahara, T. Sasaki, N. Yoneyama, N. Kobayashi, S. Fujimoto, T. Shibauchi, and Y. Matsuda, Nat. Phys. **5**, 44 (2009).
  - [28] Y.-C. He, D. N. Sheng, and Y. Chen, Phys. Rev. Lett. **112**, 137202 (2014).
  - [29] S.-S. Gong, W. Zhu, and D. N. Sheng, Sci. Rep. **4**, 6317 (2014).
  - [30] B. Bauer, L. Cincio, B. P. Keller, M. Dolfi, G. Vidal, S. Trebst, and A. W. W. Ludwig, Nat. Commun. **5**, 5137 (2014).
  - [31] Y.-C. He and Y. Chen, Phys. Rev. Lett. **114**, 037201 (2015).
  - [32] M. Barkeshli, arXiv:1307.8194.
  - [33] M. Freedman, C. Nayak, K. Shtengel, K. Walker, and Z. Wang, Ann. Phys. **310**, 428 (2004).
  - [34] V. Ivanov, Y. Qi, and L. Fu, Phys. Rev. B **89**, 085128 (2014).
  - [35] M. Levin and X.-G. Wen, Phys. Rev. B **67**, 245316 (2003).
  - [36] J. O. Fjærestad, arXiv:0811.3789.
  - [37] H. Yao and S. A. Kivelson, Phys. Rev. Lett. **99**, 247203 (2007).
  - [38] Y.-Z. Zheng, M.-L. Tong, W. Xue, W.-X. Zhang, X.-M. Chen, F. Grandjean, and G. J. Long, Angew. Chem. Int. Ed. Engl. **46**, 6076 (2007).
  - [39] M. Levin and Z.-C. Gu, Phys. Rev. B **86**, 115109 (2012).
  - [40] T. Lan and X.-G. Wen, Phys. Rev. B **90**, 115119 (2014).
  - [41] V. Elser and C. Zeng, Phys. Rev. B **48**, 13647 (1993).
  - [42] G. Misguich, D. Serban, and V. Pasquier, Phys. Rev. Lett. **89**, 137202 (2002).
  - [43] H. Yao, L. Fu, and X.-L. Qi, arXiv:1012.4470.
  - [44] B. Scharfenberger, R. Thomale, and M. Greiter, Phys. Rev. B **84**, 140404(R) (2011).
  - [45] S. Liang, B. Douçot, and P. W. Anderson, Phys. Rev. Lett. **61**, 365 (1988).
  - [46] Y. Tang, A. W. Sandvik, and C. L. Henley, Phys. Rev. B **84**, 174427 (2011).
  - [47] J. Wildeboer and A. Seidel, Phys. Rev. Lett. **109**, 147208 (2012).
  - [48] F. Yang and H. Yao, Phys. Rev. Lett. **109**, 147209 (2012).
  - [49] N. Schuch, D. Poilblanc, J. I. Cirac, and D. Pérez-García, Phys. Rev. B **86**, 115108 (2012).
  - [50] L. Wang, D. Poilblanc, Z.-C. Gu, X.-G. Wen, and F. Verstraete, Phys. Rev. Lett. **111**, 037202 (2013).
  - [51] M. P. Zaletel and A. Vishwanath, Phys. Rev. Lett. **114**, 077201 (2015).
  - [52] O. Buerschaper, S. C. Morampudi, and F. Pollmann, Phys. Rev. B **90**, 195148 (2014).
  - [53] M. Iqbal, D. Poilblanc, and N. Schuch, Phys. Rev. B **90**, 115129 (2014).